Observation of metal nanoparticles at atomic resolution in Pt-based cancer chemotherapeutics

Sheader A. A.[1,4], Varambhia A. M.[1], Fleck R. A.[2], Flatters S. J. L.[3] and Nellist P. D.[1]

[1]Department of Materials, University of Oxford
[2]Centre for Ultrastructural Imaging, Kings College London
[3]Wolfson Centre for Age-Related Diseases, Institute of Psychiatry, Psychology and Neuroscience, Kings College London
[4]Address: University of Oxford, Department of Materials, Parks Road, Oxford, OX1 3PH. Email: alex.sheader@materials.ox.ac.uk Tel: +44 1865 273657 Fax: +44 1865 283333

Abstract

The chemotherapeutics cisplatin and oxaliplatin are important tools in the fight against cancer. Both compounds are platinum complexes. Aberration-corrected scanning transmission electron microscopy using the annular dark-field imaging mode now routinely provides single atom sensitivity with atomic number contrast. Here, this imaging mode is used to directly image the platinum within the two drugs in their dried form on an amorphous carbon support film. The oxaliplatin is found to have wetted the supporting amorphous carbon, forming disordered clusters suggesting that the platinum has remained within the complex. Conversely, the cisplatin sample reveals 1.8 nm diameter metallic platinum clusters. The size and shape of the clusters does not appear to be dependent on drying rate nor formed by beam damage, which may suggest that they were present in the original drug solution.

1 Introduction

1.1 Pt-based Chemotherapy

The platinum-based antineoplastic family of chemotherapeutics (colloquially termed platins) are used extensively as first-line treatment for solid tumours. Over 50% [Johnstone et al., 2014] of

cancer treatment globally comprises, at least in part, one or more of four platinum-based drugs approved for medical use in humans.

One such drug is *cis*-[$PtCl_2(NH_3)_2$], or cisplatin. While this compound had been synthesised as early as 1845 under the moniker of Peyrone's salt, the anti-cancer potential of cisplatin was not realised until 1965, in Rosenburg's fortuitous experiments on the influence of current on cell division of Escherichia coli (*E. coli*) [Rosenberg et al., 1965].

The unexpected changes observed to the shape of the *E. coli* cells was at first thought to originate from the influence of the electric field on cellular division. However, several additional years of investigation revealed that the culprit was in fact the platinum(IV) complex *cis*-[$PtCl_2(NH_3)_2$], only present in the experiment at all due to the serendipitous combination of ammonium chloride buffer solution with the platinum electrodes. Subsequent research into the effects of platinum complexes on cells led swiftly to the idea that such compounds could be used as chemotherapeutic agents, and to the subsequent development of the first platinum-based chemotherapeutic, cisplatin.

Cisplatin is used to treat solid tumours of the bladder, cervix and lung, amongst other cancers. It is especially effective against testicular cancer, and is responsible for raising the cure rate from 5% when the drug was first approved, to over 90% today [Einhorn, 2002].

A newer member of the platin family is oxalato(trans-l-1,2-cyclohexanediamine)Pt(II), or oxaliplatin. Borne from the need for chemotherapeutics to treat cisplatin-resistant cancers (including both intrinsically resistant tumours, and those which acquire resistance over multiple courses of chemotherapy), and to reduce the extensive toxic side-effects experienced by patients [Alcindor and Beauger, 2011]. Oxaliplatin is particularly effective against colorectal tumours, against which cisplatin has no activity.

Both cisplatin and oxaliplatin share similar structures, as shown in Figure 1. Both have square-planar Pt(II) centre, with the primary difference between the two being in the replacement of the monodentate chloride groups in cisplatin with bidentate oxalate in oxaliplatin.

1.2 Annular Dark Field Scanning Transmission Electron Microscopy

In the scanning transmission electron microscope (STEM), a convergent electron beam is rastered across a specimen, and the transmitted signal collected in a number of different imaging modes. The power of STEM comes from the combination of available resolution, and the versatility of the

instrument for combination of imaging with various spectroscopic techniques. With the advent of aberration-correction optics, the modern STEM is routinely capable of producing sub-Å resolution.

The annular dark-field (ADF) detector is used in STEM to collect relatively high angles of electron scattering. An annular detector is used, and the total intensity scattered to the detector plotted as function of probe position to form an image. The ADF STEM imaging mode has two key attributes [Nellist and Pennycook, 2000]. First, the use of high angle scattering, which predominantly occurs through scattering with the atom nuclei in the sample, provides a strongly atomic number sensitive image, with the scattered intensities following an approximately $Z^{1.7}$ dependence [Krivanek et al., 2010]. This atomic number dependence allows the Pt to be readily distinguished from the other, lighter elements in the complexes. Second, the image can be described as being incoherent, which means that the total scattered intensity is relatively simply related to the number of atoms present, and allows atom counting to be performed [Van Aert et al., 2013, Varambhia et al., 2016]. In this way, zeptogram-scale weighing of small clusters in the sample is possible.

Due to the powerful combination of both high sensitivity and ease of image interpretability, ADF STEM has found great popularity in the physical sciences as a technique for examining broad ranges of inorganic materials. However, while the STEM was developed with the potential to address biological problems in mind, the technique has thus far gained relatively little purchase in the biological and soft matter fields. This is largely due to challenges associated with sample preparation and electron beam damage when compared with the heavier materials typically examined in materials science [Colliex and Mory, 1994]. Nevertheless, ADF and other STEM techniques present an intriguing prospect for addressing some highly significant biological questions [Leapman, 2004, Pan et al., 2009].

While Pt catalysts and nanoparticles have been imaged and quantified extensively using ADF STEM, few attempts have been made to apply such techniques to drugs. The Pt-based nature of the platins means they are especially suitable candidates for the first investigations of pharmaceutical compounds with ADF STEM.

2 Experimental Methods

2.1 Sample preparation

Clinical formulations of 1 mg ml^{-1} cisplatin and 5 mg ml^{-1} oxaliplatin infusion solutions (both Accord Healthcare Ltd, Harrow, UK) were prepared for STEM investigation. The vehicle of the cisplatin solution is a mixture of sodium chloride, sodium hydroxide, hydrochloric acid and water, and the oxaliplatin solution excipients are water and lactose monohydrate.

Samples were prepared by depositing 3 μl droplets directly onto lacey carbon support film on 300 mesh copper support grids (TAAB Laboratories Equipment Ltd, Aldermaston, UK). The grids were allowed to rest for 120 seconds, before being dried using the capillary mechanism of filter paper to remove excess drug suspension.

2.2 STEM methods

ADF STEM experiments were performed using a JEOL ARM-200F microscope, operated at 200kV. The microscope is equipped with probe correction for aberrations up to third order. The ADF STEM images presented were obtained using a probe semi-convergence angle of 22.48 mrad.

3 Results

3.1 Cisplatin

ADF STEM images of cisplatin are shown in Figure 2. At lower magnifications, large self-supported patches of dried drug vehicle are visible, and additional smaller regions are also observed directly on the carbon support. In both cases, increased magnification reveals the bright regions contain large quantities of metallic nanoparticles, as shown in Figure 2b. The nanoparticle size distribution is narrow, with the average diameter being 1.84nm and most particles falling within $\pm$0.2nm of this measurement.

The structure seen in Figure 3 shows clearly the [110] face-centred cubic structure typical of Pt. Measurement of the lattice spacing yields a value of 3.98$\pm$0.15Å, consistent with the spacing for bulk crystalline Pt of 3.91Å [Davey, 1925].

Other regions within the sample display evidence of very different gross large-scale morphology, as shown in Figure 4a, attributable to different local drying conditions. Nevertheless, metallic nanoparticles of ∼1.8nm average diameter are again observed. The density of nanoparticles in this region considerably higher than in the structures seen in Figure 2. However, that the average diameter remains with the bounds of the measurement error indicates that metallic nanoparticles do not arise from the drying of the drug vehicle. Working with the dried clinical formulation of cisplatin is an accepted standard for performing x-ray diffraction [Singh et al., 2012, Batista de Carvalho et al., 2011] and neutron scattering experiments [Batista de Carvalho et al., 2011].

Another possibility for the origin of such nanoparticles is beam-induced effects. It is likely that the complex would be damaged during electron irradiation, subsequently freeing the Pt to nucleate and grow into nanoparticles. Such a mechanism has been observed in other systems [Sepulveda-Guzman et al., 2007], where continued exposure drives further growth and 'ripening' of the clusters.

In order to address whether the the presence of Pt nanoparticles within the cisplatin was indeed a beam-induced effect, multi-frame acquisition was performed. The total dose was approximately 3.0×10^{10} electrons/Å^2, distributed across a 20-image stack, yielding a dose per frame of 1.5×10^9 electrons/Å^2. Frames from resulting image stack are shown in Figure 5. No ripening was observed during this process. It would seem rather unexpected that the electron exposure experienced during the first frame of imaging caused damage that would immediately result in Pt nanoparticles with a very narrow size distribution, and furthermore without there being any evidence for further damage or nanoparticle growth during the multi-frame acquisition. Nonetheless, electron-beam damage must be always be borne in mind when designing and interpreting data from the electron microscope. Figures 2, 3 and 4 were recorded using both smaller total electron dose and with a lower dose rate, suggesting that the metallic nanoparticles observed do not result from the effect of the beam.

3.2 Oxaliplatin

Identical sample preparation methods to those employed for the cisplatin solution were used to produce oxaliplatin samples, but result in very different observations. As shown in Figure 6, the latter drug displays significantly more amorphous gross morphology, likely explained by the difference in solution excipients. High-magnification images (Figure 6b) reveal non-crystalline clusters

of Pt atoms of average diameter 1.18nm, with many single Pt atoms also visible.

3.2.1 Cluster Weighing

As mentioned previously, the power of ADF STEM is that the resultant images are quantitative in nature; that is, the image intensity is directly proportional to the number of atoms in that sample region. To estimate the number of Pt atoms per small cluster, images of the type shown in Figure 6b were analysed using weighing techniques.

In order to calculate the intensity contributed to the image by a single atom, it was necessary to reduce the effects of surrounding light materials and noise on platinum quantification. This was achieved by background subtraction, with the value of the background being obtained by masking the platinum clusters and obtaining the mean intensity of the remaining image. This value was then subtracted from the complete, unmasked, image. The intensity 'weight' of a single atom was then calculated by manually selecting several individual Pt atoms far from clusters and averaging, in order to produce a representative measurement across the frame. The clusters were then re-masked, with very close neighbours being distinguished through use of appropriate watershed transforms [Meyer, 1994]. For the purposes of our analysis, clusters not wholly within the frame were excluded. The integrated intensity of each cluster was computed by summing intensities of all pixels within the background-subtracted image, and comparing with the calculated mean intensity of a single atom, to give the number of atoms per cluster N.

As the Pt clusters within the oxaliplatin are irregular in shape, simple measurement in one dimension did not accurately represent cluster size. The area, in pixels, of each cluster was re-distributed into a circular arrangement, with the 'equivalent diameter' d taken as an indication of cluster size averaged in 2D. The relationship between atoms per cluster and d is shown in Figure 7.

For a crystalline Pt nanoparticle, N would be expected to grow with particle diameter cubed:

$$N = 35.25d^3, \tag{1}$$

with the prefactor arising from considerations of Pt lattice spacing and unit cell structure, and for d in units of nanometer.

Fitting a similar power law relation to the clusters observed in oxaliplatin fails to replicate this,

with N growing instead as

$$N = 36.06d^{2.37}. \quad (2)$$

This indicates that the clusters are in fact closer to two-dimensional rather than 3D, presumably having wetted the supporting carbon film and thus appearing flattened, as observed previously in catalytic ruthenium [Varambhia et al., 2016].

The detector angles in this study were 54.1 and 276.7 mrad. Consideration of multiple scattering was not necessary for this sample because of its non-crystalline nature. The atoms in the clusters are individually resolved, so scattering from one atom cannot be then scattered by another in the cluster, an effect that was also seen in Varambhia et al. As free Pt atoms are thermodynamically driven to reduce their energy through crystallisation, the fact that the Pt clusters within oxaliplatin are not instead observed as nanoparticles (as in the case of cisplatin) is indicative that some barrier to metallic particle formation exists within oxaliplatin.

4 Discussion

Observations of nanoparticles within cisplatin have been reported previously in the literature while examining the functionalisation of single-walled carbon nanotubes as drug-delivery devices [Bhirde et al., 2009]. The recorded sizes of between 1-2nm, quantified with reference to nano-gold containing a known number of Au atoms, are consistent with those found from the experiments detailed in this article. The higher spatial resolution used in this study suggests these were also likely metallic in nature. Their observation under such different local environments lends credence to the presence of Pt nanoparticles in the pristine drug rather than being an artefact of the sample preparation methods. No such observations at atomic resolution have been made elsewhere for clinically formulated oxaliplatin.

The anti-cancer properties of both cisplatin and oxaliplatin arise from an origin common to all platins. The primary action mechanism is the induction of cytotoxicity via damage to the tumour DNA. In the case of cisplatin, chlorine leaving groups are displaced by water inside the cell cytoplasm. The aqueated form of the drug preferentially binds to guanine bases in the DNA, and allows for the formation of crosslinks, which interrupt mitosis and ultimately lead to cell death. Oxaliplatin induces cytotoxic effects again via aquation reactions of the oxalate leaving groups, and

subsequent binding to DNA, although the exact nature of the cross-linkage is not as clear as in the case of cisplatin [Alcindor and Beauger, 2011].

That the general mechanism of action is similar for both belies the observed behaviour of cisplatin and oxaliplatin at the nanoscale with ADF. Our results suggest that all the non-Pt species in the cisplatin has been stripped to enable metallic nanoparticle formation, whereas the oxaliplatin is either intact or at least sufficiently intact to prevent metal formation. The consistency of size of the nanoparticles observed in the cisplatin sample independent of the vehicle drying conditions or of the electron exposure suggests that the nanoparticles may be present prior to drying and therefore are either present during drug synthesis or can form spontaneously in the vehicle solution. Even if the drying and observation process has caused the nanoparticle formation, our work suggests that the cisplatin molecule is more susceptible to damage than oxaliplatin, which may have implications for fate of the molecule in vivo.

While all members of the platinum-based chemotherapeutic family induce unwanted secondary effects in cancer patients, typical side effects differ in both nature and severity. Peripheral neurotoxicity is associated with cisplatin treatment in as many as 50% of cases [Van Der Hoop et al., 1990], and almost all patients develop some degree of hearing loss due to the ototoxic effects of treatment [McWhinney et al., 2009].

The causal mechanisms by which such neurotoxicities arises are unclear. However, efforts to elucidate these pathways have thus far been based upon the understanding that the drug molecules remain intact until entering the cancerous cell. The evidence presented here suggests this may in fact not be the case as the observation of clusters and platinum nanoparticles may demonstrate changes within the clinical formulation of the drugs before they are ever given to patients. However, as the investigations here have been limited in scope to the examination of the pure drug only, we are unable to hypothesise about any physiological consequences which may result if this were true.

In addition, nanoparticles and nano-sized structures are themselves often toxic in their own right, being easily able to cross cellular membranes and accumulate in body tissues. Investigations of Pt nanoparticle toxicity has proved that platinum is no exception to this rule [Asharani et al., 2010]. Curiously, it has also been suggested that Pt nanoparticles may themselves exhibit an anti-cancer effect [Gao et al., 2007].

Ambiguity in the origin of the structural differences observed between these platins suggests

further work is required to more fully understand the role nanoparticles play within these drugs, particularly in vivo. Some such work has already been attempted with the use of nano-scale secondary ion mass spectrometry (NanoSIMS) on cisplatin [Legin et al., 2016], but such approaches lack the resolution to observe single platinum atoms and nanoparticles as small as those seen in the clinically formulated drug. Through direct imaging of cisplatin and oxaliplatin within tissue, some mechanisms by which these drugs damage both cancer cells and the patient, may begin to be more fully understood.

5 Conclusion

Two widely-used members of the platinum-based chemotherapeutic family, cisplatin and oxaliplatin, have been investigated using ADF STEM. Cisplatin has been revealed to contain metallic platinum nanoparticles of approximately 1.8nm diameter, potentially attributable to the loss of the organic components of the drug structure. In contrast, despite sharing structural similarities with cisplatin, the antineoplastic oxaliplatin has been shown to form non-metallic clusters, with no evidence of crystallisation within the drug. The investigation presented here demonstrates the potential for application of aberration-corrected STEM on metal-containing pharmaceuticals. Furthermore, the observation of structural change at an atomic level in such compounds suggests interesting prospects for the examination of the physiological consequences in vivo.

6 Acknowledgements

The authors would like to thank Dr G Vizcay-Barrena for technical expertise. This research was supported supported by EPSRC grant (EP/K040375/1) and DTP studentship (AAS), and a Physiological Society Research Grant 2015 awarded to SJLF.

Figures:

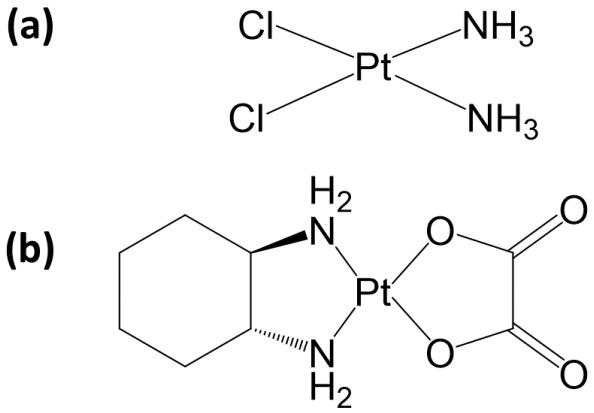

Figure 1: Chemical structure of (a) cisplatin $[Pt(NH_3)_2Cl_2]$ and (b) oxaliplatin $C_8H_{14}N_2O_4Pt$.

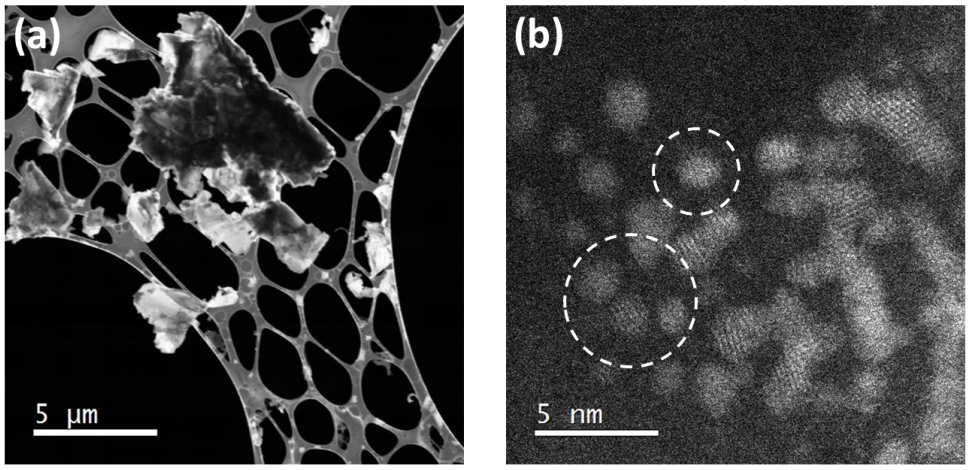

Figure 2: ADF STEM images of clinical formulation cisplatin at (a) x12k and (b) x12M magnifications. The platinum nanoparticles (circled) are of average diameter 1.84nm.

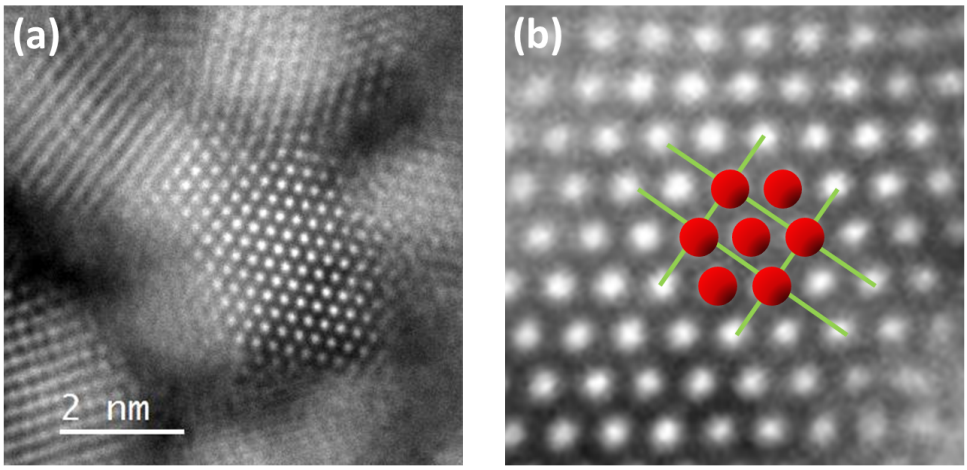

Figure 3: (a) A Pt nanoparticle. Image post-processed from multi-frame stack using Smart Align [Jones et al., 2015]. (b) Overlay of [110] face-centred cubic structure of Pt.

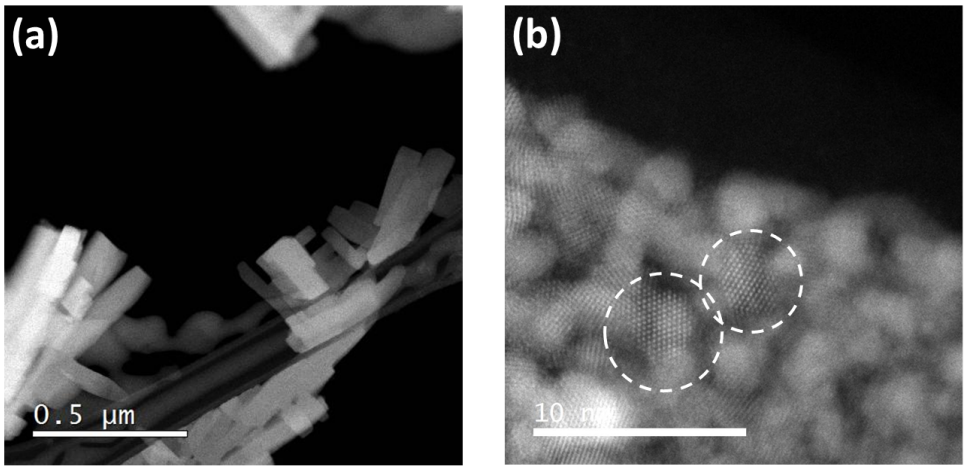

Figure 4: ADF STEM images of cisplatin at (a) x150k and (b) x12M magnifications (image post-processed from multi-frame stack using Smart Align [Jones et al., 2015]). The different morphology seen in (a) compared to Figure 1a is attributed to local differences in drying conditions. (b) shows that despite these differences, Pt nanoparticles of the same sizes are contained in this region.

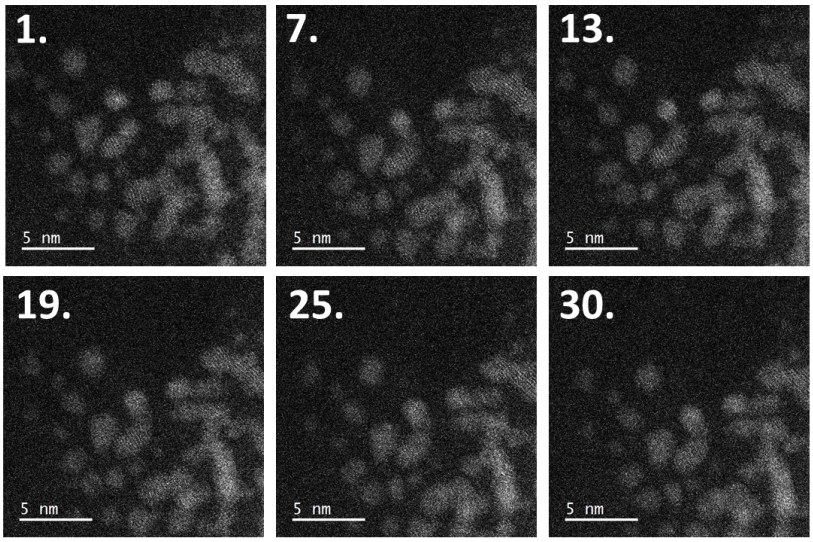

Figure 5: Frames from an image sequence. Despite drifting of the sample stage towards the lower right corner, the nanoparticle size observed remains constant at approximately 1.8nm.

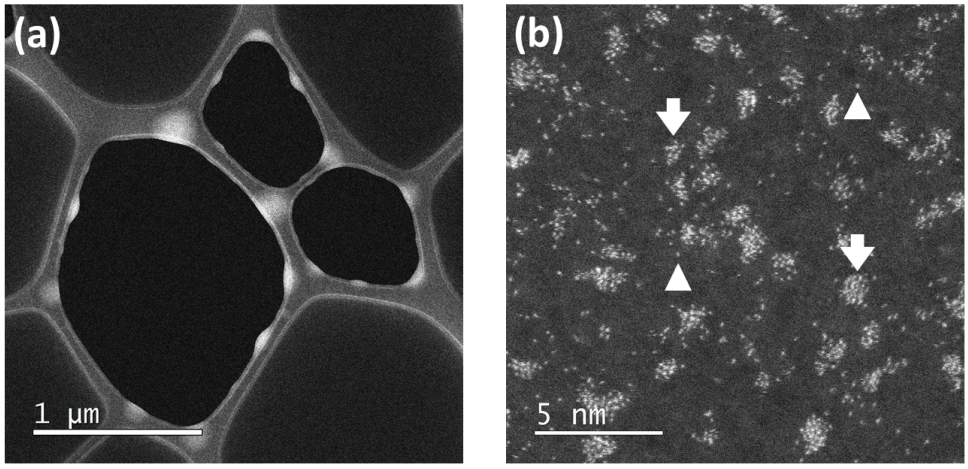

Figure 6: ADF STEM images of clinical formulation oxaliplatin at (a) x80k and (b) x12M magnification. The loose Pt clusters visible in (b) show little evidence of crystallinity, with many single atoms relative to the cisplatin shown in Figures 2 and 4.

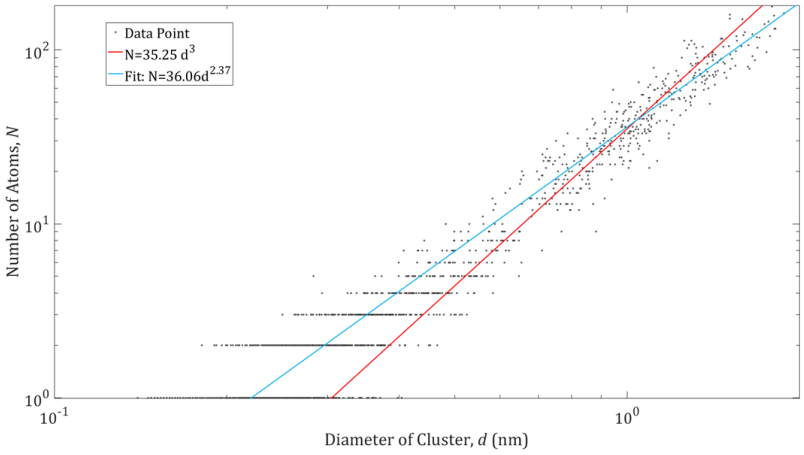

Figure 7: Number of Pt atoms plotted against cluster size in oxaliplatin. The red curve shows the theoretical relationship for spherical metallic platinum nanoparticles, while the blue curve shows the experimentally fitted curve, $N = 36.06d^{2.37}$.

References

[Alcindor and Beauger, 2011] Alcindor, T. and Beauger, N. (2011). Oxaliplatin: a review in the era of molecularly targeted therapy. *Current Oncology*, 18:18–25.

[Asharani et al., 2010] Asharani, P. V., Sethu, S., Vadukumpully, S., Zhong, S., Lim, C. T., Hande, M. P., and Valiyaveettil, S. (2010). Investigations on the structural damage in human erythrocytes exposed to silver, gold, and platinum nanoparticles. *Advanced Functional Materials*, 20(8):1233–1242.

[Batista de Carvalho et al., 2011] Batista de Carvalho, L. A. E., Marques, M. P. M., Martin, C., Parker, S. F., and Tomkinson, J. (2011). Inelastic neutron scattering study of PtII complexes displaying anticancer properties. *ChemPhysChem*, 12(7):1334–1341.

[Bhirde et al., 2009] Bhirde, A. A., Sousa, A. A., Patel, V., Azari, A. A., Gutkind, J. S., Leapman, R. D., and Rusling, J. F. (2009). Imaging the distribution of individual platinum-based anticancer drug molecules attached to single-wall carbon nanotubes. *Nanomedicine*, 4(7):763–772.

[Colliex and Mory, 1994] Colliex, C. and Mory, C. (1994). Scanning transmission electron microscopy of biological structures. *Biology of the Cell*, 80(2):175 – 180.

[Davey, 1925] Davey, W. P. (1925). Precision measurements of the lattice constants of twelve common metals. *Phys. Rev.*, 25:753–761.

[Einhorn, 2002] Einhorn, L. H. (2002). Curing metastatic testicular cancer. *Proceedings of the National Academy of Sciences*, 99(7):4592–4595.

[Gao et al., 2007] Gao, J., Liang, G., Zhang, B., Kuang, Y., Zhang, X., and Xu, B. (2007). FePt@CoS2 yolkshell nanocrystals as a potent agent to kill HeLa cells. *Journal of the American Chemical Society*, 129(5):1428–1433. PMID: 17263428.

[Johnstone et al., 2014] Johnstone, T. C., Park, G. Y., and Lippard, S. J. (2014). Understanding and improving platinum anticancer drugs - phenanthriplatin. *Anticancer research*, 34:471–6.

[Jones et al., 2015] Jones, L., Yang, H., Pennycook, T. J., Marshall, M. S. J., Van Aert, S., Browning, N. D., Castell, M. R., and Nellist, P. D. (2015). Smart align—a new tool for robust non-rigid registration of scanning microscope data. *Advanced Structural and Chemical Imaging*, 1(1):8.

[Krivanek et al., 2010] Krivanek, O. L., Chisholm, M. F., Nicolosi, V., Pennycook, T. J., Corbin, G. J., Dellby, N., Murfitt, M. F., Own, C. S., Szilagyi, Z. S., Oxley, M. P., Pantelides, S. T., and Pennycook, S. J. (2010). Atom-by-atom structural and chemical analysis by annular dark-field electron microscopy. *Nature*, 464(7288):571–574.

[Leapman, 2004] Leapman, R. D. (2004). Novel techniques in electron microscopy. *Current Opinion in Neurobiology*, 14(5):591 – 598.

[Legin et al., 2016] Legin, A. A., Theiner, S., Schintlmeister, A., Reipert, S., Heffeter, P., Jakupec, M. A., Mayr, J., Varbanov, H. P., Kowol, C. R., Galanski, M., Berger, W., Wagner, M., and Keppler, B. K. (2016). Multi-scale imaging of anticancer platinum(IV) compounds in murine tumor and kidney. *Chem. Sci.*, 7:3052–3061.

[McWhinney et al., 2009] McWhinney, S. R., Goldberg, R. M., and McLeod, H. L. (2009). Platinum neurotoxicity pharmacogenetics.

[Meyer, 1994] Meyer, F. (1994). Topographic distance and watershed lines. *Signal Processing*, 38(1):113 – 125. Mathematical Morphology and its Applications to Signal Processing.

[Nellist and Pennycook, 2000] Nellist, P. D. and Pennycook, S. J. (2000). The principles and interpretation of annular dark field z-contrast imaging. *Advances in Imaging and Electron Physics*, 113:147 – 203.

[Pan et al., 2009] Pan, Y.-H., Sader, K., Powell, J. J., Bleloch, A., Gass, M., Trinick, J., Warley, A., Li, A., Brydson, R., and Brown, A. (2009). 3d morphology of the human hepatic ferritin mineral core: New evidence for a subunit structure revealed by single particle analysis of haadf-stem images. *Journal of Structural Biology*, 166:22–31.

[Rosenberg et al., 1965] Rosenberg, B., Van Camp, L., and Krigas, T. (1965). Inhibition of cell division in escherichia coli by electrolysis products from a platinum electrode. *Nature*, 205(4972):698–699.

[Sepulveda-Guzman et al., 2007] Sepulveda-Guzman, S., Elizondo-Villarreal, N., Ferrer, D., Torres-Castro, A., Gao, X., Zhou, J. P., and Jose-Yacaman, M. (2007). In situ formation of bismuth nanoparticles through electron-beam irradiation in a transmission electron microscope. *Nanotechnology*, 18(33):335604.

[Singh et al., 2012] Singh, D. J., Lohade, A. A., Parmar, J. J., Hegde, D. D., Soni, P., Samad, A., and Menon, M. D. (2012). Development of chitosan-based dry powder inhalation system of cisplatin for lung cancer.

[Van Aert et al., 2013] Van Aert, S., De Backer, A., Martinez, G. T., Goris, B., Bals, S., Van Tendeloo, G., and Rosenauer, A. (2013). Procedure to count atoms with trustworthy single-atom sensitivity. *Phys. Rev. B*, 87:064107.

[Van Der Hoop et al., 1990] Van Der Hoop, R. G., Van Der Burg, M. E. L., Ten Huinink, W. W. B., Van Houwelingen, J. C., and Neijt, J. P. (1990). Incidence of neuropathy in 395 patients with ovarian cancer treated with or without cisplatin. *Cancer*, 66(8):1697–1702.

[Varambhia et al., 2016] Varambhia, A. M., Jones, L., De Backer, A., Fauske, V. T., Van Aert, S., Ozkaya, D., and Nellist, P. D. (2016). Quantifying a heterogeneous Ru catalyst on carbon black using ADF STEM. *Particle & Particle Systems Characterization*, 33(7):438–444.